Korean J. Chem. Eng., **31**(6), 1021-1027 (2014)
DOI: 10.1007/s11814-014-0040-4

pISSN: 0256-1115
eISSN: 1975-7220

Acid Black 172 dye adsorption from aqueous solution by hydroxyapatite as low-cost adsorbent

Gabriela Ciobanu*,†, Maria Harja*, Lacramioara Rusu, Anca Mihaela Mocanu*, and Constantin Luca***

*Gheorghe Asachi Technical University of Iasi, Faculty of Chemical Engineering and Environmental Protection, Prof. dr. docent Dimitrie Mangeron Rd., No. 63, Iasi 700050, Romania
**Vasile Alecsandri University of Bacau, Faculty of Engineering, Marasești Blvd., No. 157, Bacau 600115, Romania
(*Received 5 November 2013 • accepted 1 February 2014*)

Abstract−The Acid Black 172 dye adsorption on the uncalcined hydroxyapatite nanopowder was investigated. The hydroxyapatite prepared by wet coprecipitation method has high specific surface area of 325 m^2/g and crystal sizes smaller than 70 nm. The batch adsorption experiments revealed that under the optimum adsorption conditions (pH 3, hydroxyapatite dosage 2 g/L, initial dye concentration 400 mg/L and temperature 20 °C) the dye removal efficiency was 95.78% after 1 h of adsorption. The adsorption kinetics was best described by the pseudo-second order kinetic model. The intraparticle diffusion model shows that intraparticle diffusion is not the sole rate-limiting step; the mass transfer also influences the adsorption process in its initial period. The Langmuir isotherm model best represented the equilibrium experimental data, and the maximum adsorption capacity (q_m) was 312.5 mg/g.

Keywords: Hydroxyapatite, Acid Black 172 Dye, Adsorption, Isotherms, Kinetics

INTRODUCTION

A large number of natural and synthetic dyes are used for textile dyeing processes and also in other industries such as pharmaceutical, paper and pulp industries. Many dyes and their reaction products are very harmful due to the presence of toxic or even carcinogenic groups. The removal of dyes in the effluents is one of the major problems requiring solution by the textile industries. To solve this problem some physical (adsorption, ion-exchange, liquid-liquid extraction), chemical (oxidation, flocculation, precipitation) and biological (bacterial and fungal biosorption, biodegradation in aerobic or anaerobic conditions) methods have been attempted [1-3]. Among these, adsorption appears to be a good alternative for the effluent treatment, being a simple, non-toxic and a low-cost method [4-9].

Hydroxyapatite, $Ca_{10}(PO_4)_6(OH)_2$, is a calcium phosphate ceramic with important applications in the medicine and chemistry fields. It has been identified as a good adsorbent material for environmental processes due to its specific structure conferring ionic exchange property and adsorption affinity towards many pollutions [10]. This biomaterial has already been applied for removing heavy metal ions and organic compounds (phenols, dyes, etc.) from water [11-13].

The metal-complex dyes group is widely used in textile dyeing, being known for their high solubility and purity, and for fastness properties [14]. Unfortunately, the majority of these dyes are toxic, carcinogenic and harmful to human health due to their aromatic structure and heavy metal ions contained [15]. Acid Black 172, a water soluble Cr(VI)-complex dye, is used for the fast black dyeings on wool, nylon and leather substrates, as well as for the paper coloring. It was selected in this study as a model of anionic metal-complex dye for the adsorption experiments. However, only a limited number of studies on the Acid Black 172 removal by some adsorbents (chromium and vegetable shavings, biomass) have been found in literature [16-18].

In this study, the uncalcined hydroxyapatite nanopowder was used for the adsorption of the Acid Black 172 dye in a batch system. Still, no study has so far been focused on the adsorption ability of the hydroxyapatite for this dye. Our major objective was to investigate the effect of pH, adsorbent dose, initial dye concentration, reaction time and temperature on the adsorption capacity of the hydroxyapatite nanopowder. The adsorption behavior was analyzed based on the Langmuir and Freundlich adsorption isotherms. The experimental data were also analyzed using the pseudo-first order, pseudo-second order and intraparticle diffusion kinetic models, and the kinetic constants were calculated.

MATERIALS AND METHODS

1. Materials

The hydroxyapatite nanopowder was synthesized by wet chemical precipitation method and characterized as described elsewhere [12]. The phase composition of the hydroxyapatite powder was characterized by X-ray diffraction (XRD) by means of an X'PERT PRO MRD diffractometer (PANalytical, Netherlands) using monochromatic CuKα radiation (λ=0.15418 nm). The average crystallite size was calculated from XRD data by the Scherrer equation, selecting the peak at 2θ=25.9° for (0 0 2) reflection. The morphology and chemical composition of the sample were studied by scanning electron microscopy (SEM) coupled with energy dispersive X-ray spectroscopy (EDX) with QUANTA 200 3D microscope (FEI, Netherlands). The N_2 adsorption isotherm was recorded by a Quantachrome Nova 2200e Win2 apparatus (Quantachrome, Germany). The specific surface area was calculated by conventional Brunauer-Emmett-Teller

†To whom correspondence should be addressed.
E-mail: gciobanu03@yahoo.co.uk

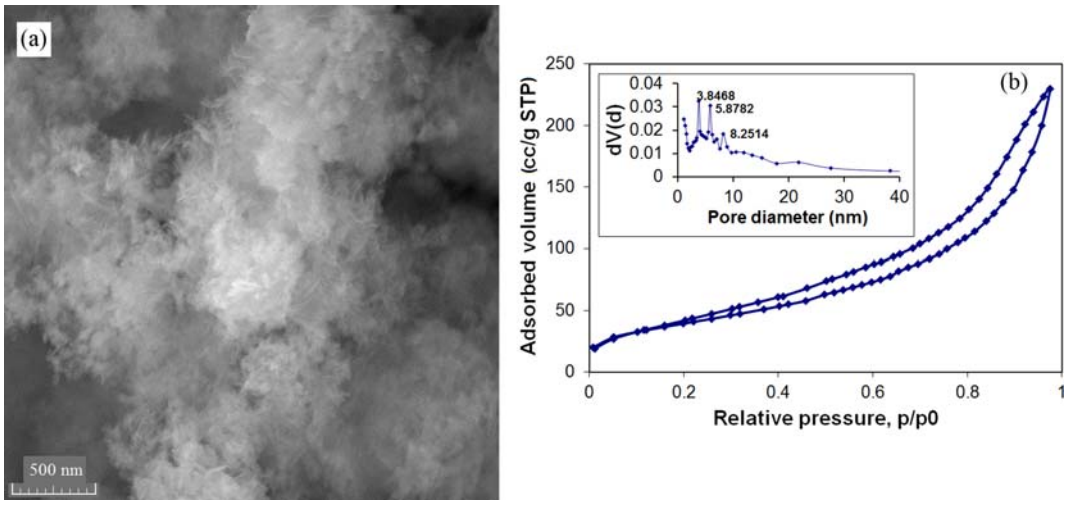

Fig. 1. SEM image (a) and adsorption-desorption isotherm with pore size distribution (b) of the uncalcined hydroxyapatite.

(BET) method, pore volume was determined by nitrogen adsorption at a relative pressure of 0.98 and pore size distribution from the adsorption isotherm by Barrett-Joyner-Halenda (BJH) method. The pH at the point of zero charge (pH_{pzc}) was determined by the pH drift method [19].

The uncalcined hydroxyapatite powder contains needle-like shape crystallites with a mean length smaller than 70 nm as seen in SEM image (Fig. 1(a)). The EDX analysis (figure not shown) confirms the presence of Ca, P, and O in the apatite crystallites. The Ca/P mole ratio was 1.682, which corresponds to the stoichiometric hydroxyapatite. The XRD pattern (figure not shown) exhibits all diffraction lines characteristic of hydroxyapatite, in good agreement with the JCPDS Data Card 09-0432 (hydroxyapatite standard). The average crystallite size calculated from XRD data by the Scherrer equation was 57 nm. The nitrogen adsorption isotherm for hydroxyapatite sample (Fig. 1(b)) exhibits a Type IV curve, characteristic of the micro-mesoporous solids. The BET surface area, pore volume and average pore diameter were 325 m^2/g, 0.357 cm^3/g and 3.84 nm, respectively. BJH analysis indicates around 72% of the hydroxyapatite surface area arises from mesopores. The point of zero charge (pH_{zpc}) for the hydroxyapatite was 7.50.

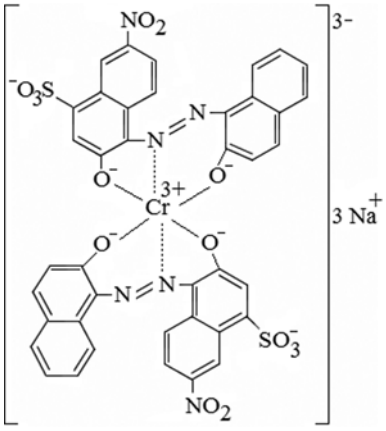

Fig. 2. The chemical structure of the acid Black 172 dye.

Acid Black 172 (**AB172**; CI 15711:1; $C_{40}H_{20}O_{14}N_6S_2Na_3Cr$; molecular weight 993 g/mol; λ_{max}=597 nm) was supplied by the Winchem Industrial Co. Ltd (China) and used without further purification. The chemical structure of AB172 dye is given in Fig. 2.

2. Preparation of Dye Solution and Determination of Dye Concentrations

A stock solution (1,000 mg/L) of AB172 dye was prepared in deionized and double distilled water. Various dye solutions with different initial concentrations were prepared by diluting the stock dye solution. The calibration curve for the AB172 dye was obtained by measuring the absorbance at 597 nm of the different dye concentrations with a UV-Vis Jasco V-550 spectrophotometer (JASCO, Japan).

3. Adsorption Experiments

Batch adsorption experiments were carried out by placing 100 mL of the corresponding AB172 dye solution and a known amount of the hydroxyapatite adsorbent into conical flasks. The flasks were agitated at 200 rpm for a given time and temperature by means of an orbital shaker. After a pre-determined contact time, each flask was removed from the shaker and the supernatant centrifuged at 5,000 rpm for 5 minutes and analyzed for dye concentration determination.

The initial pH of the AB172 dye solutions was adjusted before experiments by NaOH or HCl 0.1M solutions and controlled with a pH meter (Multi-Parameter Consort C831, Belgium).

The AB172 dye adsorption capacities at the time t (q_t, mg/g) and at equilibrium (q_e, mg/g) as well as the percentage removal (R%) referred to also as removal efficiency were calculated by means of the following relationships:

$$q_t = \frac{C_0 - C_t}{m} \cdot V \quad (1)$$

$$q_e = \frac{C_0 - C_e}{m} \cdot V \quad (2)$$

$$R\% = \frac{C_0 - C_t}{C_0} \times 100 \quad (3)$$

where C_0 is the initial concentration of dye in the solution (mg/L),

Table 1. The adsorption kinetics models

Model	Linear equation		Model parameters	Comments
Pseudo-first order kinetic model (Lagergren) [20]	$\log(q_e - q_t) = \log q_e - \frac{k_1}{2.303} \cdot t$	(4)	k_1=pseudo first-order rate constant of adsorption (min^{-1})	k_1 and q_e values were calculated from the plot of log ($q_e - q_t$) versus t
Pseudo-second order kinetic model (Ho-McKay) [21]	$\frac{t}{q_t} = \frac{1}{k_2 \cdot q_e^2} + \frac{1}{q_e} \cdot t$	(5)	k_2=pseudo-second order rate constant of adsorption (g/mg·min)	k_2 and q_e values were calculated from the plot of t/q_t versus t
Intraparticle diffusion model (Weber-Morris) [22]	$q_t = k_{id} \cdot t^{1/2} + c$	(6)	k_{id}=intraparticle diffusion rate constant ($mg/g \cdot min^{1/2}$); c=intercept (mg/g)	k_{id} and c values were calculated from the plot of q_t versus $t^{1/2}$

Table 2. The adsorption isotherms

Isotherm	Linear equation		Model parameters	Comments
Langmuir [23]	$\frac{t}{q_t} = \frac{1}{k_2 \cdot q_e^2} + \frac{1}{q_e} \cdot t$	(7)	q_m=maximum adsorption capacity (mg/g); K_L=Langmuir equilibrium constant (L/mg)	q_m and K_L values were calculated from the plot of $1/q_e$ versus $1/C_e$
Freundlich [24]	$\log q_e = \log K_F + \frac{1}{n_F} \cdot \log C_e$	(8)	K_F=Freundlich equilibrium constant ($mg^{(1-1/n)} \cdot L^{1/n}/g$); n_F=Freundlich constant or adsorption intensity	K_F and n_F values were calculated from the plot of log q_e versus log C_e

C_t and C_e are the concentration of dye (mg/L) in the solution at any time t (min) and at equilibrium, respectively, V is the volume of solution (L) and m is the mass of the adsorbent (g). All experiments were run three times and the average results were used to data analysis.

To evaluate the AB172 dye adsorption ability by the uncalcined hydroxyapatite, the effects of the pH (2-13), adsorbent dose (0.2-5 g/L), initial dye concentration (50-400 mg/L), contact time (0-24 h) and temperature (20-60 °C) on the dye adsorption were studied.

4. Adsorption Kinetics Models

Kinetic studies are required for optimizing different operation conditions for the AB172 dye adsorption on hydroxyapatite. The adsorption process order and the rate constant were estimated by applying the pseudo-first order kinetic, pseudo-second order kinetic and intraparticle diffusion models (Table 1), and the model with higher correlation coefficient (R^2) was chosen.

5. Adsorption Isotherms

Adsorption isotherms describe the relationship between the amount of AB172 dye adsorbed on the hydroxyapatite and the dye concentration in the solution at equilibrium. The results obtained from the equilibrium adsorption experiments were analyzed according to the Langmuir and Freundlich isotherm models (Table 2), and the model with higher correlation coefficient (R^2) was chosen.

RESULTS AND DISCUSSION

1. Adsorption Experiments

1-1. Effect of Initial pH

The effect of the initial pH of solution on the AB172 dye adsorption onto uncalcined hydroxyapatite was examined in the pH range of 2-13. As seen in Fig. 3, the percentage removal (R%) was higher in acidic pH media and lower in basic pH media. For removing the AB172 dye, the maximum adsorption was found at pH=3 with a dye percentage removal of about 95.78%. Hence, the pH value of 3 was chosen as the optimal pH for further AB172 dye adsorption experiments.

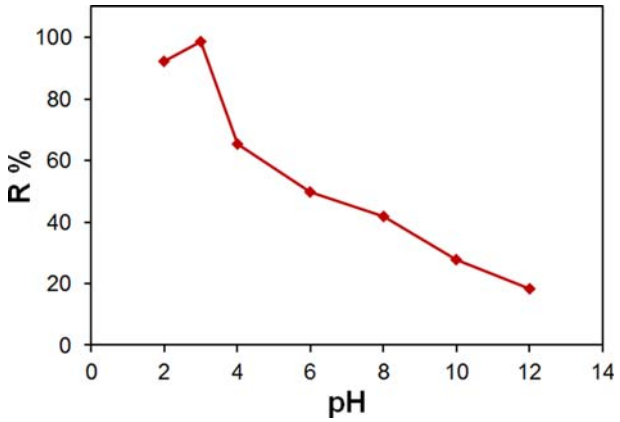

Fig. 3. Initial pH influence on AB172 dye adsorption onto uncalcined hydroxyapatite (initial dye concentration 400 mg/L, adsorbent dose 2 g/L, contact time 1 h and temperature 20 °C).

The pH of the AB172 dye solution and the point of zero charge (pH_{pzc}) of the hydroxyapatite were important controlling parameters in the adsorption process. The pH effect on the dye adsorption is related to the amphoteric nature of the hydroxyapatite surface and also to the anionic nature of the AB172 dye. The pH_{pzc} value determined for hydroxyapatite sample was 7.50. For pH values lower than pH_{pzc}, the hydroxyapatite presents a positive surface charge due to the protonation process, in good agreement with literature data [25]. Therefore, the AB172 (anionic) dye adsorption on the hydroxyapatite may be explained to proceed via electrostatic attraction between the positively charged surface of the hydroxyapatite and the negatively charged groups of the dye. The decrease in the pH of the solution increases the electrostatic attraction between the dye and adsorbent, which results in increased adsorption of AB172 dye. The decrease in the dye adsorption for the solution pH lower than 3.0 might be caused by the dissolution of the hydroxyapatite at very low pH values [25]. Similar observations were previously re-

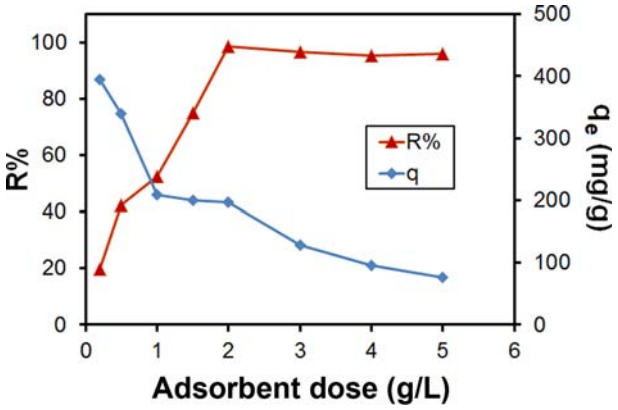

Fig. 4. Adsorbent dose influence on AB172 dye adsorption onto uncalcined hydroxyapatite (initial pH 3, initial dye concentration 400 mg/L, contact time 1 h and temperature 20 °C).

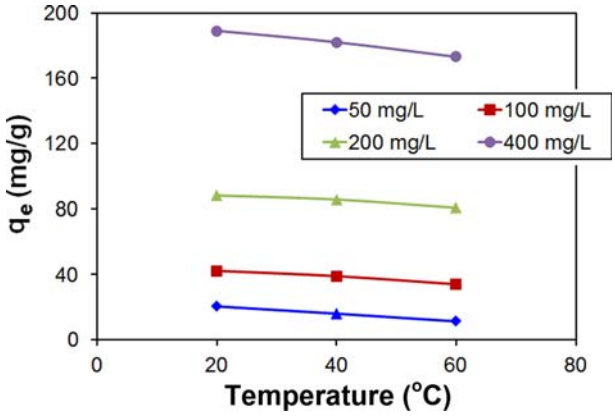

Fig. 6. Effect of temperature on AB172 dye adsorption onto uncalcined hydroxyapatite (initial pH 3, adsorbent dose 2 g/L and contact time 1 h).

ported for the AB172 dye adsorption on other adsorbents [16,18].

1-2. Effect of Adsorbent Dose

The effect of adsorbent dose on the removal of AB172 dye by the uncalcined hydroxyapatite sample was evaluated over the 0.2-5 g/L range of the adsorbent. Fig. 4 shows the dye percentage removal and adsorption capacity as a function of the hydroxyapatite nanopowder dosage under given conditions. The dye percentage removal is seen to increase with increasing adsorbent dose, and the maximum was attained at 2 g/L adsorbent dose. These results could be attributable to the increased surface area of the adsorbent and availability of more adsorption sites. Above 2 g/L of adsorbent dose, the extent of adsorption is increasingly slowed down. Therefore, 2 g/L adsorbent dose was used for further experiments. Also, from Fig. 4 it is observed that the dye adsorption capacity decreases with increase in hydroxyapatite dose. This is due to the splitting effect of flux (concentration gradient) between adsorbate and adsorbent.

1-3. Effect of Contact Time and Initial Dye Concentration

The effect of the contact time and initial dye concentration (50-400 mg/L) on the AB172 dye adsorption onto hydroxyapatite is presented in Fig. 5. A rapid increase occurs for the first 20 min and it then proceeds slowly until reaching equilibrium within 1 h for the whole studied range of the initial dye concentrations. The rapid adsorption at the initial contact time is due to the availability of the positively charged surface of the adsorbent, which led to electrostatic adsorption of the anionic AB172 dye from the solution at pH 3. The rapid adsorption rate has significant practical importance, which ensures high efficiency and cost-effectiveness. From the contact time study, 1 h is enough to achieve equilibrium and hence the subsequent adsorption experiments were conducted with 1 h contact time. An increase of the initial dye concentration leads to an increase in the adsorption capacity. Thus, as the initial dye concentration increases from 50 to 400 mg/L, the adsorption capacity of the dye onto adsorbent changes from 24.33 to 193.55 mg/g. Similar results have been reported in the literature for the removal of dyes and organic compounds by various adsorbents [16-18,26].

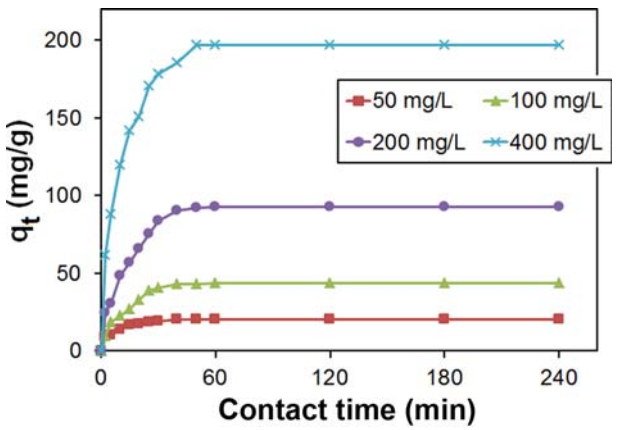

Fig. 5. Initial dye concentration influence on AB172 dye adsorption onto uncalcined hydroxyapatite (initial pH 3, adsorbent dose 2 g/L and temperature 20 °C).

1-4. Effect of Temperature

The temperature effect on the adsorption of AB172 dye on hydroxyapatite sample was studied at three different temperatures (20, 40 and 60 °C). As shown in Fig. 6, the adsorption capacity decreases with increasing temperature for the whole studied range of the initial dye concentrations and the maximum adsorption capacity value being obtained at 20 °C. This indicates that the AB172 dye adsorption on uncalcined hydroxyapatite sample is controlled by an exothermic process.

2. Adsorption Kinetic Study

The kinetics of AB172 dye adsorption onto uncalcined hydroxyapatite is required for selecting optimum operating conditions for the full-scale batch process. The kinetic parameters, which are helpful for the prediction of adsorption rate, give important information for designing and modeling the adsorption processes.

The dye adsorption process in a porous solid can be separated into three stages: (1) dye diffusion through the solution to the external surface of the adsorbent (film mass transfer or boundary layer diffusion of solute molecules), (2) dye diffusion within the pores or capillaries of the adsorbent internal structure to the adsorption sites, and (3) dye uptake. The last step is assumed to be rapid while steps (1) and (2) are the rate determining steps, either singly or in combination [27].

To investigate the mechanism of the AB172 dye adsorption on uncalcined hydroxyapatite and potential rate-controlling steps (such as external mass transfer, intraparticle diffusion and adsorption pro-

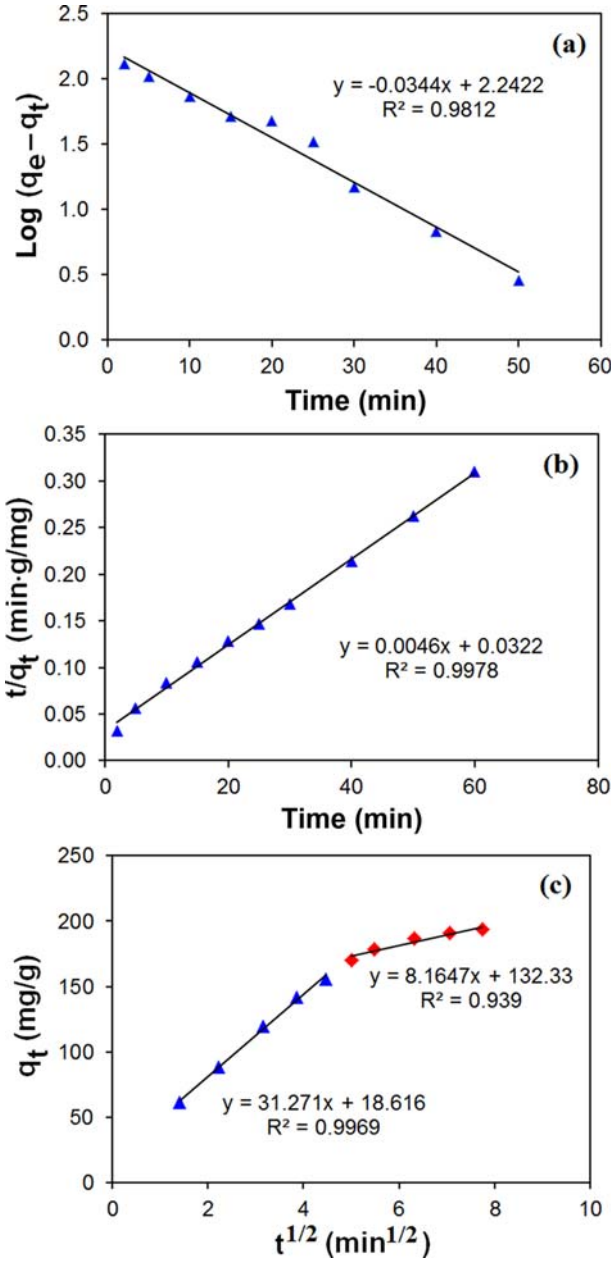

Fig. 7. The pseudo-first order (a), pseudo-second order (b) and intraparticle diffusion (c) kinetic models for AB172 dye adsorption onto uncalcined hydroxyapatite (initial pH 3, adsorbent dose 2 g/L, initial dye concentration 400 mg/L and temperature 20 °C).

cesses), the mass transfer (intraparticle diffusion model) and kinetic (pseudo-first order and pseudo-second order kinetic models) models have been used to test the experimental data.

The kinetic parameters for the above models were calculated from corresponding linear plots presented in Fig. 7, and the results are listed in Table 3. The pseudo-second order kinetic model was most suitable for explanation of dye adsorption process mechanism due to highest value of correlation coefficient (R^2). Also, the calculated equilibrium sorption capacity ($q_{e,calc}$) was close to values of experimental data ($q_{e,exp}$) for the whole studied range of the initial dye concentrations suggest the applicability of pseudo-second order kinetic model to these adsorption systems. The results indicated that boundary layer resistance was not a rate-limiting step since dye adsorption followed pseudo-second order kinetics [28].

Usually, the adsorption rate is governed by liquid phase mass transport or intraparticle mass transport. To get information about the diffusion mechanism, the kinetic results were analyzed by the intraparticle diffusion model. Fig. 7(c) presents the linear plot of the intraparticle diffusion model. It shows two separate regions, revealing that the process is governed by two steps: the initial part is attributed to the bulk diffusion, while the final part to the intraparticle diffusion. The first linear portion (phase I) at all concentrations and for the first 20 min, can be attributed to the immediate utilization of the most readily available adsorbing sites on the adsorbent surface. Phase II may be attributed to very slow diffusion of the AB172 dye from the hydroxyapatite surface site into the inner pores. Thus, the initial portion of AB172 dye ion adsorption by hydroxyapatite may be governed by the initial intraparticle transport of the dye controlled by surface diffusion process and the latter part controlled by pore diffusion. The values of $k_{id(I)}$ and $k_{id(II)}$ (diffusion rate constants for the phases I and II, respectively) obtained from the slope of linear plots are listed in Table 3. The results obtained indicate that intraparticle diffusion controls the adsorption rate. At the same time, external mass transfer resistance cannot be neglected, although this resistance is only significant for the initial period of time (first 20 min). Also, the values of the intercept (c) give an idea about the thickness of the boundary layer (Table 3), i.e., the larger the intercept the greater is the boundary layer effect. Similar observations were previously reported for the AB172 dye adsorption on other adsorbents [16,18].

3. Adsorption Study

For solid-liquid systems, the adsorption isotherm is very important in describing the adsorption behavior. In this work, we evaluated two well-known models of Langmuir and Freundlich isotherm. These isotherms were obtained at 20, 40, and 60 °C. The linear forms of the Langmuir and Freundlich adsorption isotherms are given in Fig. 8, and the adsorption isotherm constants are listed in Table 4. The best fitted model was selected based on the determination of the correlation coefficient (R^2). As seen in Table 4, the R^2 values of the Langmuir isotherm model were higher than those of the Freundlich model, meaning that the experimental equilibrium data are better explained by the Langmuir model. This finding supports the assumption that the AB172 dye is adsorbed as a homogeneous monolayer on hydroxyapatite particle sites. Also, the results indicated that maximum adsorption capacity of hydroxyapatite decreased with increasing temperature.

The essential characteristic of the Langmuir equation can be expressed in terms of a dimensionless factor R_L (Hall separation factor), which can be calculated in the following equation [29]:

$$R_L = \frac{1}{1 + K_L \cdot C_0} \tag{9}$$

where K_L is the Langmuir constant (L/mg) and C_0 is the initial dye concentration in the solution (mg/L). R_L values indicate that the adsorption process is irreversible (R_L=0), favorable (0<R_L<1), linear (R_L=1) or unfavorable (R_L>1) [30]. In the present study, the R_L values (calculated for the initial dye concentration of 400 mg/L) were 0.0383, 0.0973 and 0.0718 at 20 °C, 40 °C and 60 °C, respectively. R_L values are situated within the range of 0<R_L<1, which indicates that the

Table 3. Kinetic parameters for AB172 dye adsorption on uncalcined hydroxyapatite (initial pH 3, adsorbent dose 2 g/L and temperature 20 °C)

Kinetic model	Parameter		Initial dye concentration (mg/L)			
			50	100	200	400
	$q_{e,\,exp}$ (mg/g)		24.33	48.44	95.57	193.55
Pseudo-first order	$q_{e,\,calc}$ (mg/g)		29.47	50.25	102.18	174.66
	k_1 (min^{-1})		0.0691	0.0640	0.0689	0.0792
	R^2		0.9343	0.9738	0.9793	0.9812
Pseudo-second order	$q_{e,\,calc}$ (mg/g)		22.22	52.08	103.09	217.39
	k_2 (g/mg·min)		0.0090361	0.0018770	0.0013716	0.0006551
	R^2		0.9972	0.9929	0.9920	0.9971
Intraparticle diffusion	I	$k_{id(I)}$ (mg/g·$min^{1/2}$)	3.6645	6.4465	16.7400	31.2710
		$c_{(I)}$ (mg/g)	1.1970	1.1963	7.5693	18.6160
		$R^2_{(I)}$	0.9682	0.9676	0.9896	0.9969
	II	$k_{id(II)}$ (mg/g·$min^{1/2}$)	2.4297	4.1784	6.8332	8.1647
		$c_{(II)}$ (mg/g)	6.1191	17.0280	44.1880	132.3300
		$R^2_{(II)}$	0.9500	0.9361	0.9121	0.9390

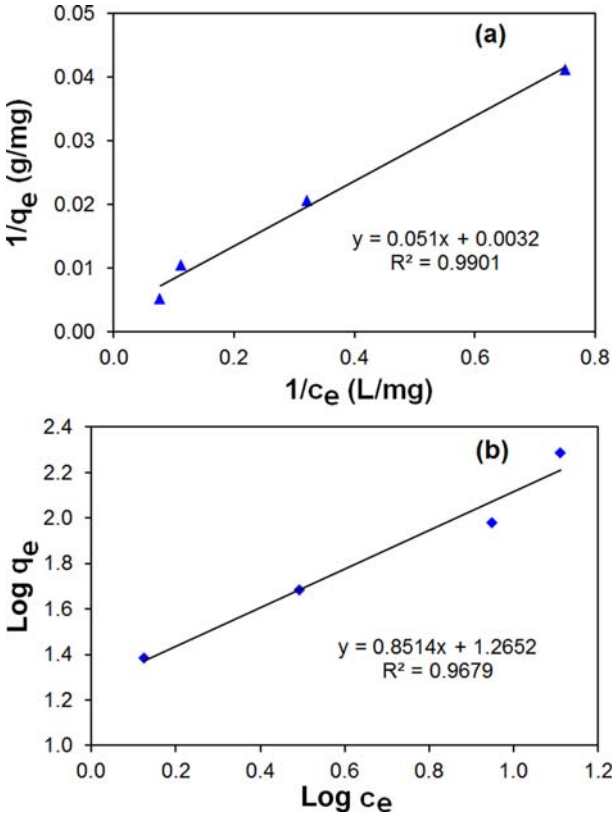

Fig. 8. Langmuir (a) and Freundlich (b) isotherms for AB172 dye adsorption on uncalcined hydroxyapatite (initial pH 3, adsorbent dose 2 g/L and contact time 1 h).

adsorption of AB172 dye on the uncalcined hydroxyapatite is favorable.

The maximum adsorption capacity (q_m) values obtained for the present system in comparison with those reported earlier for sorption of AB172 dye onto various adsorbents (Table 5) revealed that the uncalcined nanohydroxyapatite was effective adsorbent in the AB172 dye removing.

Finally, the results obtained in this study suggest that uncalcined nanohydroxyapatite acts an efficient adsorbent for the removal of AB172 dye from aqueous solutions, being an alternative for eliminating the AB172 dye from industrial wastewaters.

Table 4. Adsorption isotherm constants for the adsorption of AB172 dye on uncalcined hydroxyapatite (initial pH 3, adsorbent dose 2 g/L and contact time 1 h)

Parameter	Temperature (°C)		
	20	40	60
Langmuir isotherm:			
q_m (mg/g)	312.50	270.27	178.57
K_L (L/mg)	0.0627	0.0232	0.0323
R^2	0.9901	0.9840	1.9040
Freundlich isotherm:			
K_F ($mg^{(1-1/n)} \cdot L^{1/n}/g$)	18.4162	7.2127	7.5788
n_F	1.1745	1.2086	1.3806
$1/n_F$	0.8514	0.8274	0.7243
R^2	0.9679	0.9294	0.9358

Table 5. Comparison of adsorption capacity (q_m) of AB172 dye with various adsorbents

Type of adsorbent	q_m (mg/g)	Reference
Chromium shavings	172.4	[16]
Vegetable shavings	111.1	[16]
Pseudomonas sp. strain DY1 (biomass)	2828.02	[17]
Penicillium YW 01 (biomass)	185.19	[18]
Uncalcined nanohydroxyapatite	312.5	Present work

CONCLUSIONS

Uncalcined nanohydroxyapatite has been used successfully as

adsorbent for removing Acid Black 172 dye from aqueous solution. The uncalcined hydroxyapatite used has a crystal size smaller than 70 nm and a high specific surface area of 325 m^2/g.

The batch adsorption experiments followed the influence of various parameters such as pH, adsorbent dose, initial dye concentration, contact time and temperature on the adsorption process. In the batch system, the maximum dye uptake of about 95.78% was noticed at pH 3 and 20 °C. The adsorption process reached equilibrium after 1 h of contact time.

The kinetic studies indicate that the dye adsorption follows a pseudo-second order kinetic model with intraparticle diffusion as one of the rate determining steps. The Langmuir isotherm model was found to provide the best fit of the equilibrium experimental data. The adsorption process was spontaneous and decreased with increase in temperature, showing the exothermic nature of the adsorption. The Acid Black 172 dye adsorption on hydroxyapatite may be explained to proceed via the electrostatic attraction between the positively charged surface of the hydroxyapatite and the negatively charged groups of the dye.

The results indicate that the uncalcined nanohydroxyapatite possessed good adsorption ability towards Acid Black 172 dye and can be used as a low cost adsorbent for removing the dye from wastewater.

REFERENCES

1. A. Bhatnagar and A. K. Minocha, *Indian J. Chem. Technol.*, **13**, 203 (2006).
2. C. Liu, H. Xu, H. Li, L. Liu, L. Xu and Z. Ye, *Korean J. Chem. Eng.*, **28**, 1126 (2011).
3. P. Pandit and S. Basu, *Environ. Sci. Technol.*, **38**, 2435 (2004).
4. P. Luo, B. Zhang, Y. Zhao, J. Wang, H. Zhang and J. Liu, *Korean J. Chem. Eng.*, **28**, 800 (2011).
5. L. Liu, Y. Wan, Y. Xie, R. Zhai, B. Zhang and J. Liu, *Chem. Eng. J.*, **187**, 210 (2012).
6. M. Shirmardi, A. H. Mahvi, B. Hashemzadeh, A. Naeimabadi, G. Hassani and M. V. Niri, *Korean J. Chem. Eng.*, **28**, 1126 (2011).
7. P. Luo, Y. Zhao, B. Zhang, J. Liu, Y. Yang and J. Liu, *Water Res.*, **44**, 1489 (2010).
8. M. Harja, G. Buema, D. M. Sutiman, C. Munteanu and D. Bucur, *Korean J. Chem. Eng.*, **29**, 1735 (2012).
9. G. Ciobanu and G. Carja, *Desalination*, **250**, 698 (2010).
10. J. C. Elliott, *Structure and chemistry of the apatites and other calcium orthophosphates*, Elsevier Press, Amsterdam (1994).
11. G. Ciobanu, D. Ignat, G. Carja and C. Luca, *Environ. Eng. Manage. J.*, **8**, 1347 (2009).
12. G. Ciobanu, S. Ilisei, M. Harja and C. Luca, *Sci. Adv. Mater.*, **5**, 1090 (2013).
13. Y. Hannachi, N. A. Shapovalov and A. Hannachi, *Korean J. Chem. Eng.*, **27**, 152 (2010).
14. F. Beffa and G. Back, *Rev. Prog. Color. Relat. Top.*, **14**, 33 (1984).
15. J. S. Bae and H. S. Freeman, *Dyes Pigm.*, **73**, 126 (2007).
16. G. Zengin, H. Ozgunay, E. M. Ayan and M. M. Mutlu, *Pol. J. Environ. Stud.*, **21**, 499 (2012).
17. L. N. Du, B. Wang, G. Li, S. Wang, D. E. Crowley and Y. H. Zhao, *J. Hazard. Mater.*, **205-206**, 47 (2012).
18. Y. Yang, G. Wang, B. Wang, Z. Li, X. Jia, Q. Zhou and Y. Zhao, *Bioresour. Technol.*, **102**, 828 (2011).
19. M. N. Khan and A. Sarwar, *Surf. Rev. Lett.*, **14**, 461 (2007).
20. S. Lagergren, *K. Sven. Vetenskapsakad. Handl.*, **24**, 1 (1898).
21. Y. S. Ho and G. McKay, *Chem. Eng. J.*, **70**, 115 (1998).
22. W. J. Weber Jr. and J. C. Morris, *J. Sanitary Eng. Div. Proceed. Am. Soc. Civil Eng.*, **89**, 31 (1963).
23. I. Langmuir, *J. Am. Chem. Soc.*, **38**, 2221 (1916).
24. H. M. F. Freundlich, *Z. Phys. Chem.*, **57**, 385 (1906).
25. I. S. Harding, N. Rashid and K. A. Hing, *Biomaterials*, **26**, 6818 (2005).
26. M. Shirzad-Siboni, S. J. Jafari, M. Farrokhi, J. K. Yang, *Environ. Eng. Res.*, **18**, 247 (2013).
27. A. Özer, G. Akkaya and M. Turabik, *J. Hazard. Mater.*, **135**, 355 (2006).
28. X. J. Xiong, X. J. Meng and T. L. Zheng, *J. Hazard. Mater.*, **175**, 241 (2010).
29. K. R. Hall, L. C. Eagleton, A. Acrivos and T. Vermeule, *Ind. Eng. Chem. Fund.*, **5**, 212 (1966).
30. T. W. Weber and R. K. Chakravorti, *J. Am. Inst. Chem. Eng.*, **20**, 228 (1974).